

Sulfur K-edge XANES analysis of natural and synthetic basaltic glasses: Implications for S speciation and S content as function of oxygen fugacity

Pedro J. Jugo^{a,*}, Max Wilke^b, Roman E. Botcharnikov^c

^a *Laurentian University, Department of Earth Sciences, Sudbury, ON, Canada P3E 2C6*

^b *Helmholtzzentrum Potsdam, Deutsches GeoForschungsZentrum (GFZ), Telegrafenberg, Potsdam D-14473, Germany*

^c *Institut für Mineralogie, Leibniz Universität, Hannover D-30167, Germany*

Received 8 February 2010; accepted in revised form 18 July 2010; available online 25 July 2010

Abstract

XANES analyses at the sulfur K-edge were used to determine the oxidation state of S species in natural and synthetic basaltic glasses and to constrain the fO_2 conditions for the transition from sulfide (S^{2-}) to sulfate (S^{6+}) in silicate melts. XANES spectra of basaltic samples from the Galapagos spreading center, the Juan de Fuca ridge and the Lau Basin showed a dominant broad peak at 2476.8 eV, similar to the spectra obtained from synthetic sulfide-saturated basalts and pyrrhotite. An additional sharp peak at 2469.8 eV, similar to that of crystalline sulfides, was present in synthetic glasses quenched from hydrous melts but absent in anhydrous glasses and may indicate differences in sulfide species with hydration or presence of minute sulfide inclusions exsolved during quenching. The XANES spectra of a basalt from the 1991 eruption of Mount Pinatubo, Philippines, and absarokitic basalts from the Cascades Range, Oregon, USA, showed a sharp peak at 2482.8 eV, characteristic of synthetic sulfate-saturated basaltic glasses and crystalline sulfate-bearing minerals such as hauyne. Basaltic samples from the Lamont Seamount, the early submarine phase of Kilauea volcano and the Loihi Seamount showed unequivocal evidence of the coexistence of S^{2-} and S^{6+} species, emphasizing the relevance of S^{6+} to these systems. XANES spectra of basaltic glasses synthesized in internally-heated pressure vessels and equilibrated at fO_2 ranging from FMQ – 1.4 to FMQ + 2.7 showed systematic changes in the features related to S^{2-} and S^{6+} with changes in fO_2 . No significant features related to sulfite (S^{4+}) species were observed. These results were used to construct a function that allows estimates of $S^{6+}/\Sigma S$ from XANES data. Comparison of $S^{6+}/\Sigma S$ data obtained by S K α shifts measured with electron probe microanalysis (EPMA), $S^{6+}/\Sigma S$ obtained from XANES spectra, and theoretical considerations show that data obtained from EPMA measurements underestimate $S^{6+}/\Sigma S$ in samples that are sulfate-dominated (most likely because of photo-reduction effects during analysis) whereas $S^{6+}/\Sigma S$ from XANES provide a close match to the expected theoretical values. The XANES-derived relationship for $S^{6+}/\Sigma S$ as a function of fO_2 indicates that the transition from S^{2-} to S^{6+} with increasing fO_2 occurs over a narrower interval than what is predicted by the EPMA-derived relationship. The implications for natural systems is that small variation of fO_2 above FMQ + 1 will have a large effect on S behavior in basaltic systems, in particular regarding the amount of S that can be transported by basaltic melts before sulfide saturation can occur.

© 2010 Elsevier Ltd. All rights reserved.

1. INTRODUCTION

Sulfur is a trace element in silicate melts (typically below 0.2 wt%) but it is a key element in several magmatic processes. For example, sulfide phases control the behavior of most metals of economic interest either because of the

* Corresponding author. Tel.: +1 705 675 1151x2106; fax: +1 705 675 4898.

E-mail address: pjugo@laurentian.ca (P.J. Jugo).

chalcophile nature of these metals (e.g., Cu, Ni, Co) or because of the association of highly siderophile elements (Ru, Rh, Pd, Re, Os, Ir, Pt, Au) with sulfide phases (e.g., Mitchell and Keays, 1981; Alard et al., 2000). Some of these chalcophile and siderophile elements (e.g., Pb, Re, Os) are often used as tracers of petrogenetic processes (e.g., Roy-Barman et al., 1998; Rehkamper et al., 1999; Hart and Gaetani, 2006). Therefore, understanding the factors controlling sulfide saturation in silicate melts has received significant attention (Haughton et al., 1974; Mavrogenes and O'Neill, 1999; O'Neill and Mavrogenes, 2002; Clemente et al., 2004; Liu et al., 2007; Li and Ripley, 2009). Sulfur (as SO₂) is an essential magmatic volatile component, along with H₂O and CO₂, and some explosive volcanic eruptions can release large amounts of sulfur into the stratosphere significantly affecting global climate. The Permian–Triassic extinction, for example, has been linked to major sulfur emissions caused by the eruption of basalts in the Siberian Traps large igneous province (e.g., Campbell et al., 1992; Rampino and Self, 1992; Renne et al., 1995; Self et al., 1996; Reichow et al., 2009).

Several aspects make S a complex element to understand in magmatic systems. First, S may occur as sulfide (S²⁻), sulfate (S⁶⁺), or a combination of both in silicate melts (e.g., Carroll and Rutherford, 1988; Wallace and Carmichael, 1994; Paris et al., 2001). Second, sulfite (S⁴⁺), as SO₂, is the dominant S species in volcanic gases, followed by H₂S and minor amounts of S₂ and COS (e.g., Carroll and Webster, 1994; Symonds et al., 1994). Third, as for other multivalent elements (e.g., Fe) variations in *f*O₂ determine the oxidation state and the proportion of coexisting species; however, the transition from S²⁻ to S⁶⁺ in silicate melts occurs over a very narrow *f*O₂ interval (roughly between FMQ and FMQ + 2) whereas the transition from Fe²⁺ to Fe³⁺ expands over 16 log *f*O₂ units (Jayasuriya et al., 2004). Because of the relatively high S contents required to form anhydrite (or an immiscible sulfate liquid) from basaltic silicate melts, S behaves mostly as an incompatible element when it is present as S⁶⁺ in mafic magmas. In contrast, relatively low S contents (as S²⁻) are required to reach sulfide saturation (e.g., Carroll and Rutherford, 1985, 1987; Luhr, 1990; Jugo et al., 2005a; Liu et al., 2007; Moune et al., 2009). For silicate melts containing a combination of S⁶⁺ and S²⁻, Jugo (2009) predicted that small changes in *f*O₂ strongly affect the S content at sulfide saturation (SCSS) and the changes are expected to occur in *f*O₂ interval that is relevant for magmas in several tectonic regimes.

Since the development of electron microprobe techniques to estimate the sulfate proportion (S⁶⁺/ΣS) in silicate glasses by the shift in energy of the S Kα X-ray emissions (Carroll and Rutherford, 1988; Wallace and Carmichael, 1994), several studies have documented the dominance of sulfate species in some subduction-related magmas (Matthews et al., 1999; De Hoog et al., 2004; Rowe et al., 2007; Vigouroux et al., 2008). The development of X-ray Absorption Near Edge Structure (XANES) spectroscopy as a tool to identify different S species (Li et al., 1995; Paris et al., 2001; Mckeown et al., 2004; Fleet, 2005; Fleet et al., 2005) has provided significant insights into the complexities of S behavior in silicate melts. One significant aspect is the

potential presence of several S species in silicate glasses. Although Paris et al. (2001) suggested that S⁶⁺ and S²⁻ were the only S species relevant to S dissolution in silicate melts, Métrich et al. (2002) documented the presence of S⁴⁺ in basaltic glasses and discussed the implications of this additional species for S transfer from the silicate melt to a magmatic volatile phase. However, Wilke et al. (2008) showed that S⁴⁺ detected with XANES is an analytical artifact and the result of photo-reduction of sulfate species in the quenched glasses due to beam–sample interaction during prolonged microprobe exposure or during high-flux XANES analyses. Although Métrich et al. (2009) showed evidence that S⁴⁺ was present in Fe-free synthetic glasses, they concluded that the proportion of S⁴⁺, compared to S²⁻ and S⁶⁺, is insignificant in silicate melts. Thus, it is reasonable to assume that S behavior in silicate melts can be described in terms of S²⁻ and S⁶⁺, which allows for the development of models to explain how S content at sulfide saturation (SCSS) or sulfate content at anhydrite saturation (SCAS) change in silicate melts with changes in *f*O₂ (Jugo, 2009). Métrich et al. (2009) highlighted another potential problem: self-oxidation of sulfide to sulfate during quenching by simultaneous reduction of ferric iron to ferrous iron according to the reaction:



Métrich et al. (2009) argued that the real (S⁶⁺/S²⁻) is unquenchable because electron transfer is expected to happen very fast and may occur even below the glass transition temperature, and concluded that (S⁶⁺/S²⁻) or S⁶⁺/ΣS (as more commonly determined by EPMA) measured in silicate glasses are not reliable indicators of S⁶⁺/ΣS in the silicate melt at magmatic conditions.

The purpose of this contribution is to present XANES analyses of natural and experimental samples and use them to: (a) provide information about S speciation in natural magmatic systems; (b) show that S⁶⁺ and S²⁻ can coexist in silicate melts (both natural and experimental) and that features related to S⁴⁺ are absent or insignificant; (c) show that S⁶⁺/ΣS is quenchable; (d) demonstrate that S⁶⁺/ΣS obtained by EPMA tend to overestimate S⁶⁺/ΣS, particularly in oxidized samples; (e) derive a method to estimate S⁶⁺/ΣS from XANES data; and (f) refine models for the SCSS and SCAS in basaltic melts that account for the presence of S⁶⁺ and S²⁻ in silicate melts.

2. SAMPLES AND METHODS

Natural samples from several localities were analyzed (Table 1). The samples include basaltic submarine glasses from the Galapagos Spreading Center, Juan de Fuca Ridge, Lamont Seamounts, Lau Basin, Loihi Seamounts, basanites from the early submarine phase of Kilauea volcano, melt inclusions in olivine from the western Oregon Cascades (Quartzville basalt), and melt inclusions in hornblende from the 1991 eruption of Mount Pinatubo (of andesitic composition as documented in De Hoog et al. (2004)). Experimental samples are quenched glasses of basaltic composition synthesized in piston-cylinder (Jugo et al., 2005a,b) and internally-heated pressure vessels (Tables 2 and 3).

Table 1
Summary of locations and references for the natural samples analyzed.

Sample	Locality	References
D1-4G	Juan de Fuca Ridge	[1]
1540-4	Galapagos Spreading Center, 95.5°W	[1]
10-3-1	Lau Basin	[1]
1560-1843Z	Lamont Seamounts	[1]
1567-2019Z	Lamont Seamounts	[1]
1564-1857	Lamont Seamounts	[1]
F2-2	Lamont Seamounts	[1]
KK-15-4	Loihi Seamount	[1]
KK-15-5	Loihi Seamount	[1]
KK-16-1	Loihi Seamount	[1]
KK-19-21	Loihi Seamount	[1]
KK-21-1	Loihi Seamount	[1]
KK-29-10	Loihi Seamount	[1]
S508	Kilauea volcano (early submarine phase)	[2]
P-bas-1	Pinatubo basalt from 1991 eruption	[3]
QV04-3B	Quartzville basalt (Oregon Cascades)	[4]

References: [1]: Wallace and Carmichael (1992, 1994); [2]: Sisson (2003); [3]: de Hoog et al. (2004); [4]: Rowe et al. (2007).

The oxygen fugacity in experiments conducted in internally-heated pressure vessels was nominally fixed using Ar–H₂ gas mixtures; fH_2 was controlled with a Shaw mem-

brane (e.g., Berndt et al., 2002; Botcharnikov et al., 2005). Thus, the fO_2 in each experiment depends on hydrogen diffusion through the capsule walls (and osmotic equilibration between charge and the pressure media), water activity, and water dissociation. Water activity was calculated using the expression $aH_2O = H_2O^{melt}/H_2O^{max}$, where H_2O^{melt} is water content of the melt in an individual experiment and H_2O^{max} is the water solubility in given basaltic melt at given P and T . In the calculation we assumed that the activity coefficient of H₂O in water-rich basaltic melts is close to unity. This assumption is expected to be valid for basaltic compositions at 200 MPa total pressure and close to water saturation (e.g., Botcharnikov et al., 2005; Shishkina et al., in press). The fO_2 was calculated using thermodynamic considerations on water dissociation reaction at given T , P and fH_2 :

$$\log fO_2^{(capsule)} = \log fO_2^{(at aH_2O=1)} + 2 \log(aH_2O) \quad (2)$$

where $\log fO_2^{(capsule)}$ is oxygen fugacity of each experiment; $\log fO_2^{(at aH_2O=1)}$ is the oxygen fugacity expected in the capsule with water activity equal to one at given T , P and fH_2 ; aH_2O is water activity in the capsule.

XANES spectra at the S K-edge were collected at the European Synchrotron Radiation Facility (ESRF; Grenoble, France) using the scanning X-ray microscope (SXM) of the ID21 (X-ray microscopy) beamline. The beamline uses a fixed-exit, Si(111) double-crystal monochromator to scan the energy of the incoming beam and two plane-par-

Table 2
Summary of conditions and references for experimental samples analyzed.

Sample	Composition and run conditions	Notes, References
PJ-004	Basaltic sulfide-saturated, 1300 °C, 1 GPa, anhydrous	[1]
PJ-026	Basaltic sulfate-saturated, 1300 °C, 1 GPa, anhydrous	[1]
PJ-052	Basaltic sulfate-saturated, 1300 °C, 1 GPa, anhydrous	[1]
SB-5	Basaltic, internally-heated vessel, 200 MPa, 1050 °C, hydrous	FMQ + 2.7
SB-6	Basaltic, internally-heated vessel, 200 MPa, 1050 °C, hydrous	FMQ + 0.9
SB-15	Basaltic, internally-heated vessel, 200 MPa, 1050 °C, hydrous	FMQ + 1.8
SB-19	Basaltic, internally-heated vessel, 200 MPa, 1050 °C, hydrous	FMQ + 1.6
SB-35	Basaltic, internally-heated vessel, 200 MPa, 1050 °C, hydrous	FMQ + 1.3
SB-36	Basaltic, internally-heated vessel, 200 MPa, 1050 °C, hydrous	FMQ – 0.1
SB-41	Basaltic, internally-heated vessel, 200 MPa, 1050 °C, hydrous	FMQ – 1.4 ^a

[1] Jugo et al. (2005a,b).

^a Sample SB-41 was synthesized in the presence of graphite; the fO_2 for this sample was determined using the model of Churakov and Gottschalk (2003) for fluid mixtures.

Table 3
Composition (in wt%) of experiments synthesized in internally-heated pressure vessels (determined by EPMA).

Sample	SiO ₂	TiO ₂	Al ₂ O ₃	FeO	MnO	MgO	CaO	Na ₂ O	K ₂ O	P ₂ O ₅	S	Total
SB-5	47.48	1.61	16.52	7.90	0.02	5.44	9.90	3.49	1.95	0.54	0.60	95.44
SB-6	45.72	1.70	15.67	9.56	0.18	5.48	10.31	3.33	1.88	0.53	0.28	94.64
SB-15	45.64	1.69	15.73	9.46	0.14	5.34	10.25	3.40	1.90	0.56	0.60	94.71
SB-19	45.41	1.71	15.39	9.90	0.17	5.21	10.15	3.43	1.89	0.49	0.52	94.27
SB-21	45.42	1.70	15.33	9.90	0.28	5.25	10.12	3.18	1.88	0.34	0.47	93.87
SB-30	44.99	1.66	15.19	9.91	0.16	5.24	10.12	3.27	1.90	0.52	0.47	93.43
SB-35	45.06	1.67	15.22	9.70	0.12	5.40	10.13	3.20	1.83	0.47	0.41	93.21
SB-36	45.33	1.68	15.69	8.38	0.13	5.39	10.09	3.32	1.78	0.58	0.12	92.50
SB-41	47.97	1.97	17.39	7.95	0.17	3.68	7.90	4.28	2.58	0.72	0.07	94.68

allel mirrors with an adjustable angle of incidence to reject higher harmonics. The energy of the monochromator was calibrated to the position of the white line of the spectrum of gypsum (2482.84 eV). The incident beam intensity was measured using a photodiode and the spectra were collected in fluorescence mode using an energy dispersive Si-drift chamber solid-state detector. Two types of beam were used: (a) beams ranging from 50 to 200 μm in diameter (“broad” beams) were obtained using pinholes of the desired diameter on Au foil of 100 μm thickness to collimate the beam before the sample; (b) focused beams of $0.4 \times 0.8 \mu\text{m}$ were obtained using an arrangement consisting of a Fresnel zone plate and a central stop (to focus the beam to sub-micrometer sections without significant loss in beam flux) in combination with an order-selecting aperture to reject undesired harmonics (Susini et al., 2002). The XANES spectra were acquired by continuously scanning the monochromator and changing the gap of the undulator to produce an energy step size of 0.23 eV. The samples were typically scanned quickly from 2450 to 2550 eV (400 steps) with a dwell time of 0.1 s. The quick-scans were stacked until an appropriate signal-to-noise ratio was achieved (typically in groups of 40 scans). Spectra were normalized by fitting the energy region before the edge with a polynomial function and subtracting this function to the spectra to eliminate the background. The edge jump was normalized to unity by fitting an arctangent and a Gaussian function to the spectra. Crystalline material was used as reference to define the features of the main S species: a hauyne crystal from the Eifel volcanic field (Germany) was used as reference for sulfate, a synthetic pyrrhotite formed upon quenching of an immiscible sulfide liquid (Jugo et al., 2005a) was used as reference for sulfide and reagent-grade sodium sulfite powder was used as reference for sulfite. Samples that had been analyzed previously by electron probe microanalysis (EPMA) were re-polished to expose fresh surfaces and to avoid the presence of sulfite species caused by beam-sample interaction (Wilke et al., 2008).

3. RESULTS

3.1. Reference material

Fig. 1 shows the results of the XANES analysis of the reference material used to define the position and characteristic of the features associated with S^{2-} , S^{4+} and S^{6+} species. Two features characterize the S^{2-} spectrum of the synthetic pyrrhotite: a broad peak at 2476.8 eV and a sharp peak at 2469.8 eV. A single peak at 2482.8 eV that has very high intensity relative to the normalized edge jump characterizes the S^{6+} spectrum of hauyne. The spectrum of the sulfite sample (synthetic Na-sulfite) has two peaks: a small peak at 2478.3 eV and a sharp peak at 2482.8 eV. The second peak matches the position and shape of the sulfate peak and was interpreted to be the result of partial oxidation of the sodium sulfite to sodium sulfate (this is unavoidable because crystalline sulfite is very unstable and oxidizes very fast). Therefore, the peak at 2478.3 eV was used as the only criterion to establish the presence of sulfite in the samples analyzed. This assignment is consistent to previous work on S speciation

by XANES (Métrich et al., 2002, 2009; McKeown et al., 2004; Fleet, 2005; Fleet et al., 2005; Backnaes et al., 2008).

3.2. Reduced, sulfide-dominated samples

Fig. 2 shows the XANES results spectra of sulfide-dominated samples. The XANES spectra of the crystalline sulfide and sulfate reference materials are also shown. Sample PJ-004 is a synthetic, sulfide-saturated basaltic glass and shows the characteristic broad peak centered at 2476.8 eV observed in pyrrhotite. However, the relative intensity of this peak is higher in the basaltic glass than in the Fe-sulfide reference. At lower energies (ca. 2470–2471 eV) a clear shoulder is visible. The spectrum of the sample from Lau Basin looks very similar to the synthetic one. Two further natural glass samples (Juan de Fuca, Galapagos) show an additional sharp feature at 2469.8 eV, which is quite similar in position to the one found in pyrrhotite but different in intensity. Data from Fleet (2005) indicate that this low energy feature in the XANES spectra depends strongly on the neighboring atoms of S. For crystalline model compounds, its position shifts in energy depending on whether S is present as CaS, MgS or FeS. Only FeS shows a peak at 2469.8 that is clearly separated from the edge. In addition, the sample D1-4G (Juan de Fuca) shows a small shoulder at 2482.8 eV that is consistent with minor amounts of sulfate in the sample.

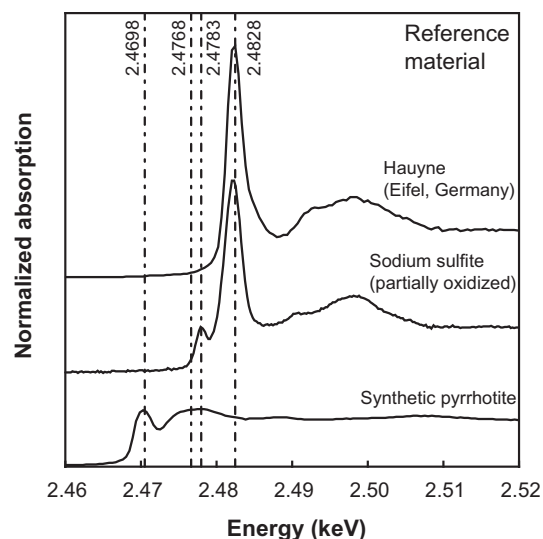


Fig. 1. XANES spectra used to define the peak positions and intensities for sulfide (S^{2-}), sulfite (S^{4+}) and sulfate (S^{6+}) species. Synthetic pyrrhotite is from quenched sulfide liquid. Hauyne was collected from the Eifel volcanic field (Germany). Reagent-grade sodium sulfite was used as sulfite reference but because the material was significantly oxidized, the sulfite peak likely has a much lower intensity than if the reference material were pure sulfite. Suitable sulfite reference material without oxidation was not available for this study. The vertical lines indicate the energy of the main features: 2469.8 eV for a sharp sulfide peak; 2476.8 eV as the center of a broad sulfide peak; 2478.3 eV for the sulfite peak; 2482.8 eV for the sulfate peak.

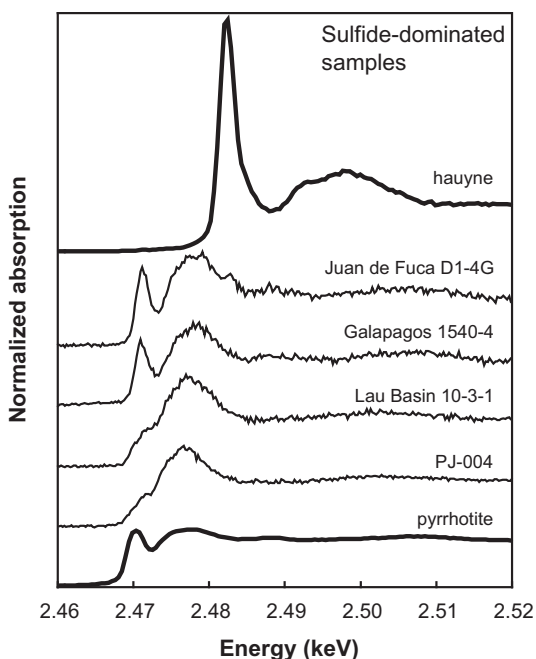


Fig. 2. XANES spectra of sulfide-dominated samples. The spectra of the sulfide (pyrrhotite) and sulfate (hauyne) reference material are shown for reference. The broad sulfide peak centered at 2478.3 eV is common for all spectra; it is higher in the glass samples than in the sulfide reference. The sharp peak at 2469.8 eV shows marked variability among the analyzed glass samples, being almost absent in the experimental glass (PJ-004) and the Lau basin sample but well defined in the Juan de Fuca and Galapagos samples. Of the samples analyzed only the Juan de Fuca (D1-4G) sample shows some small features corresponding to sulfite and sulfate.

3.3. Oxidized, sulfate-dominated samples

Fig. 3A and B summarize the results of sulfate-dominated samples. The experimental samples in Fig. 3A are all anhydrous and sulfate-saturated. All the samples showed the intense 2482 eV peak characteristic of sulfate species. No significant features associated with other S species were recorded. Fig. 3B shows the results for sulfate-dominated natural samples. The spectra of sample QV04-3B are from three different melt inclusions in olivine. The spectrum of sample P-bas-1 is from a melt inclusion in hornblende (see De Hoog et al. (2004) for further details). The signal to noise ratio in these samples is lower than in the synthetic samples (Fig. 3A) because the S content is much lower. However, the spectra show that sulfate is the dominant species in all the samples. No sulfide species were detected in QV04-3B. A feature resembling the sharp peak at 2469.8 eV is present in the spectrum of P-bas-1 but the lack of a feature matching the broad peak at 2476.8 eV is an indication that no sulfide is present. The samples shown in Fig. 3B have a small peak at 2478.3 eV, corresponding to sulfite. However, all the melt inclusion samples were analyzed with a focused beam (because of their small size) and the presence of small amounts of sulfite is most likely caused by photo-reduction of sulfate during analysis, which is unavoidable when a focused beam is used (Wilke et al., 2008).

3.4. Natural samples with coexisting sulfide and sulfate species

XANES spectra in natural samples from the Lamont Seamount (Fig. 4), the early phase of Kilauea (Fig. 5) and the Loihi Seamount (Fig. 6) showed coexistence of S^{2-} and S^{6+} . No S^{4+} species was detected in these glasses. The S^{2-} component of the spectra is similar in all the samples, showing the broad peak at 2476.8 eV and a minor peak at 2469.8 eV. The intensities of the S^{2-} features are essentially identical in the samples. However, the intensities of the S^{6+} peak differ. In the Lamont Seamount samples the intensity of the S^{6+} peak is similar to the intensity of the broad S^{2-} peak and there is no significant variation among the samples. In the Kilauea samples the intensity of the S^{6+} peak is higher and more variable than in the Lamont Seamount samples. The samples from the Loihi Seamount showed the largest variability in the intensity of the S^{6+} peak. Sample KK-15-4 was an anomaly and showed only S^{2-} features.

3.5. Synthetic basaltic glasses with coexisting sulfide and sulfate species

XANES spectra of water-bearing basalts synthesized at 200 MPa and 1050 °C under different fO_2 conditions illustrate the effect of fO_2 on the intensity of S^{6+} and S^{2-} features. Fig. 7A shows the spectra of four basaltic glasses. The spectra are overlapped rather than stacked to illustrate the differences in the intensities of the S^{6+} peak. Fig. 7B is a detail of the spectra in Fig. 7A scaled to show the variations in the features corresponding to S^{2-} in the basaltic glasses. Both figures illustrate the increase in sulfide species with decreasing fO_2 . At FMQ + 2.7 (sample SB-5), no S^{2-} was detected and S is present only as S^{6+} . The spectrum for SB-5 is similar to the spectra of basaltic and andesitic glasses synthesized in piston-cylinder at higher pressures (Fig. 3A). At FMQ + 1.6 (sample SB-19) S^{6+} is still dominant but minor S^{2-} was inferred, based on comparison with the shoulder of sample SB-5 (Fig. 7B). The spectra of samples synthesized at FMQ + 1.3 (sample SB-35) and at FMQ + 0.9 (sample SB-6) show a progressive decrease in the relative intensity of the S^{6+} peak with decreasing fO_2 that is matched by a progressive increase in the relative intensities of the S^{2-} features. The most reduced sample (SB-41), which equilibrated at $fO_2 = FMQ - 1.4$ does not show the separated peak at 2469.8 eV, in contrast to sulfide-saturated basaltic glasses synthesized in the piston-cylinder (Fig. 2 sample PJ-004), which shows the feature although with very low intensity. Comparison of the intensities at 2476.8 eV consistently indicates a systematic decrease of this sulfide-related feature with decreasing fO_2 .

4. DISCUSSION

4.1. Dominant S species in silicate melts

Sulfide (S^{2-}) and sulfate (S^{6+}) were the dominant species in the spectra of all samples analyzed. Some spectra (e.g., Fig. 3B) show the presence of small features characteristic

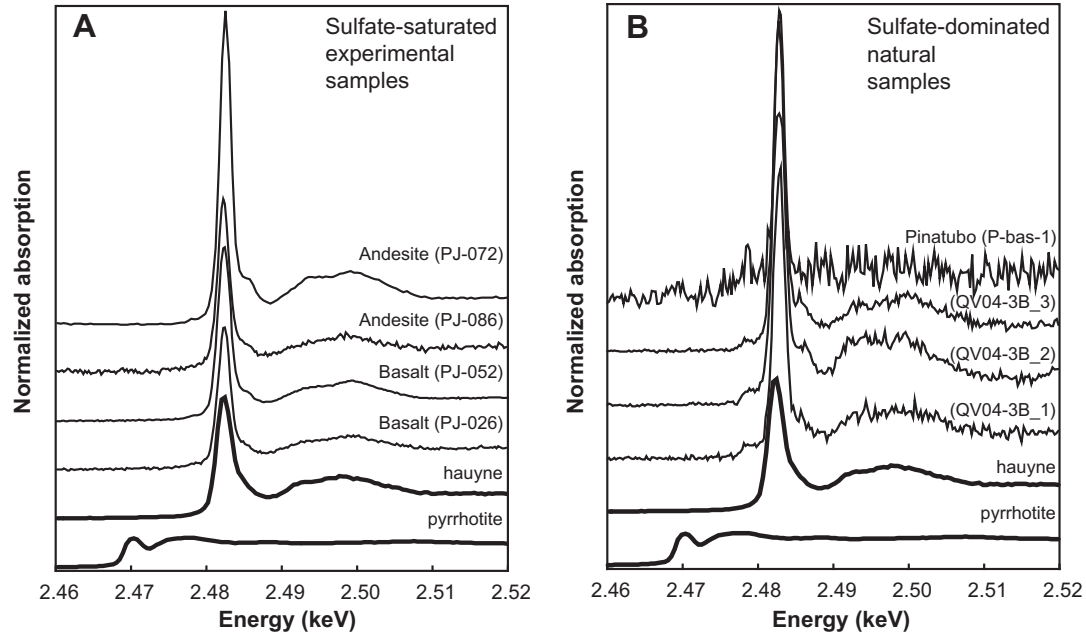


Fig. 3. XANES spectra of sulfate-dominated samples. (A) Spectra of anhydrous sulfate-saturated samples synthesized in a piston-cylinder at 1 GPa and 1300 °C. (B) Spectra of arc-related melts inclusions. P-bas-1 is a melt inclusion in hornblende from the products of the 1991 eruption of Mount Pinatubo (de Hoog et al., 2004); the three spectra of the QV04-3B series are spectra of three different melt inclusions in olivine from a cinder cone in the Oregon Cascades (Rowe et al., 2007). The spectrum of the Pinatubo sample is noisy because of low S content in the sample and small sample volume. All four spectra show dominantly sulfate, clearly no indication of sulfide and some features suggesting sulfite. However, sulfite in these samples is likely an analytical artifact.

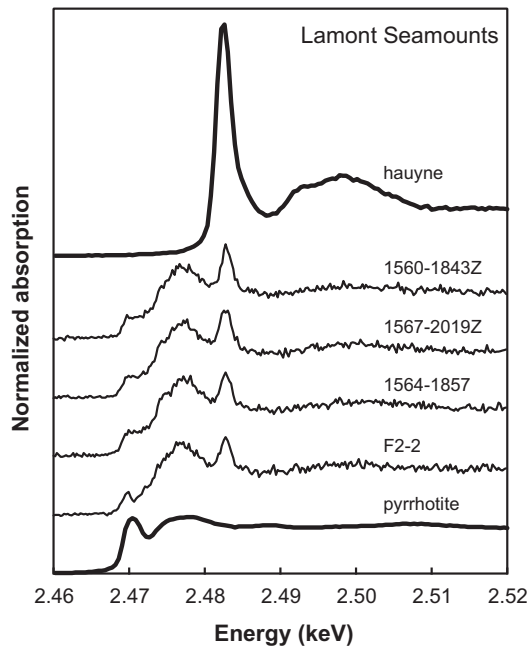


Fig. 4. XANES spectra of basalts from the Lamont Seamounts samples. The four samples analyzed show roughly identical patterns, clearly indicating coexistence of sulfide and sulfate species and lack of sulfite species, in the glasses. The sulfate peak intensity relative to the edge jump is very small compared to the sulfate reference material or glass samples containing only sulfate (cf. Fig. 3) whereas the sulfide peaks are roughly as intense as in the sulfide-only samples (Fig. 2) indicating higher proportion of sulfide to sulfate.

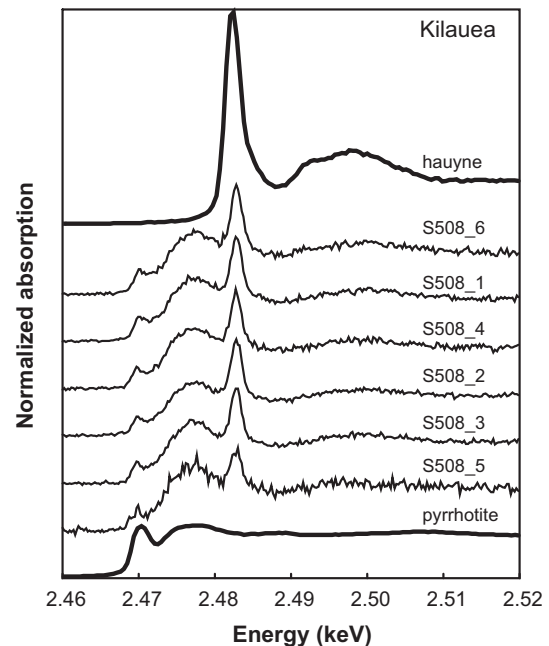


Fig. 5. XANES spectra of basalts from samples of the early eruptive phase of Kilauea. The general shape of the spectra is similar to that of the samples from the Lamont Seamounts, indicating coexistence of sulfide and sulfate species. However, the relative intensity of the sulfate peak in these samples is more variable, which indicates variations in the sulfate/sulfide in the glasses.

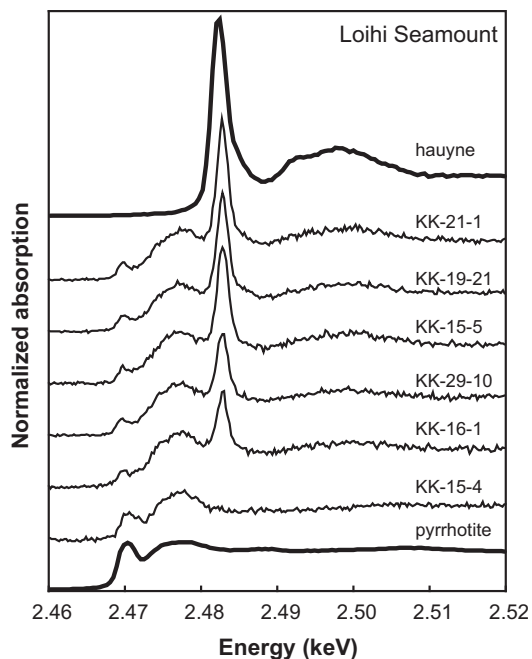


Fig. 6. XANES spectra of basalts from the Loihi Seamount samples. This suite also shows coexistence of sulfide and sulfate species (except for sample KK-15-4, which has no sulfate features). Compared with the suite of samples from the Lamont Seamounts and Kilauea the relative intensity of the sulfate peak indicates that these samples have even higher sulfate/sulfide and that the proportion is more variable.

of sulfite (S^{4+}). Wilke et al. (2008) showed that beam-sample interaction produces S^{4+} by photo-reduction of S^{6+} , especially under high photon flux. Because the melt inclusion samples were analyzed with a focused beam, we interpret the S^{4+} features in these samples as analytical artifacts. Even if S^{4+} were assumed to be real, the small intensity of the S^{4+} peaks in the analyzed glasses indicates that, at best, the amount of S^{4+} present is minor compared to the amounts of S^{2-} and S^{6+} . Thus, we suggest that S^{4+} can be safely ignored when modeling the behavior of S in silicate melts (although S^{4+} is the dominant oxidation state of S in the volatile phases exsolving from the melt). The results shown here are consistent with the results of Paris et al. (2001) who first proposed that only S^{2-} and S^{6+} are relevant in silicate melts. Backnaes et al. (2008) also found that S^{2-} and S^{6+} were the only S species present in silicate glasses, even in samples synthesized in equilibrium with SO_2 gas and sodium sulfite. Backnaes et al. (2008) concluded that in their experiments S^{4+} disproportionated into S^{2-} and S^{6+} . Métrich et al. (2009) documented sulfite species in Fe-free and Fe-poor silicate glasses. However, they state that “the solubility of S^{4+} is insignificant at low pressure” and “it is likely to remain insignificant at higher pressures” (Métrich et al., 2009, p. 2395). Furthermore, in the basaltic glasses synthesized at various fO_2 (Fig. 7) only sulfide and sulfate species were detected. However, a conclusive answer regarding whether S^{4+} is present or not in silicate melts will require *in situ* XANES analysis of molten silicate as suggested by Backnaes et al. (2008).

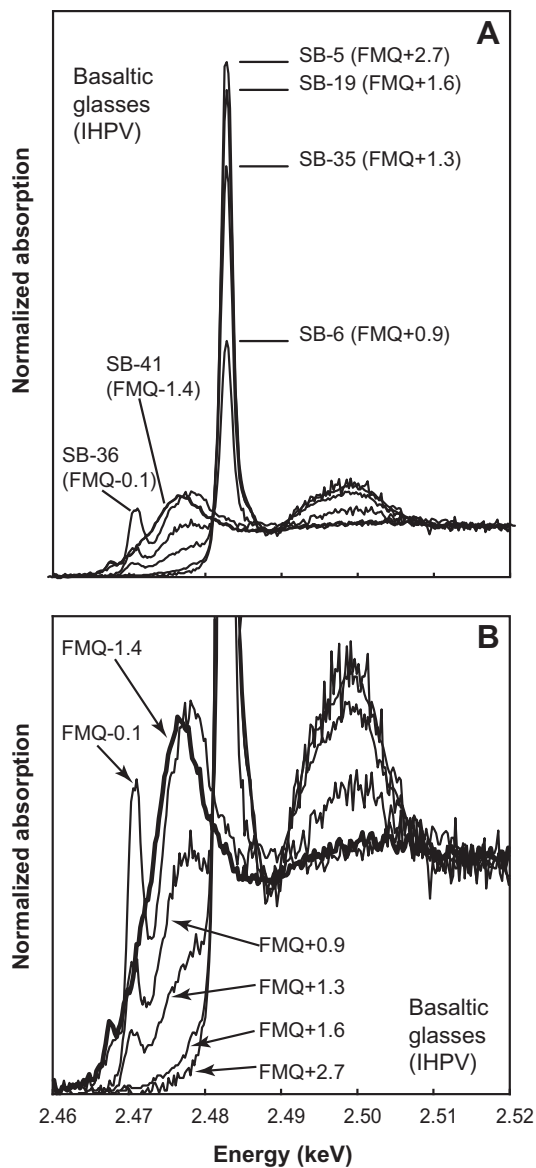


Fig. 7. XANES spectra of hydrous basaltic glasses synthesized in internally-heated pressure vessels. The samples are overlapped rather than stacked to better compare the relative intensity of the sulfide and sulfate features. (A) Complete spectra highlighting the increase in the intensity of the sulfate peak with increasing fO_2 . (B) Detail of the region corresponding to the sulfide feature showing how the intensity of the sulfide features increase with decreasing fO_2 .

4.2. Estimates of $S^{6+}/\Sigma S$ from XANES spectra

The signals of the normalized spectra at the energy positions for sulfide and sulfate were used to estimate $S^{6+}/\Sigma S$. The signal window for sulfide (henceforth $I(S^{2-})$) was integrated between 2475.7 and 2480 eV. The signal window for sulfate (henceforth $I(S^{6+})$), was integrated between 2481.5 and 2484 eV. To define the relationship between the relative variation of the two signal windows and $S^{6+}/\Sigma S$, a sequence of spectra (Fig. 8A) was calculated by combining the spectra of a completely oxidized glass and a completely reduced

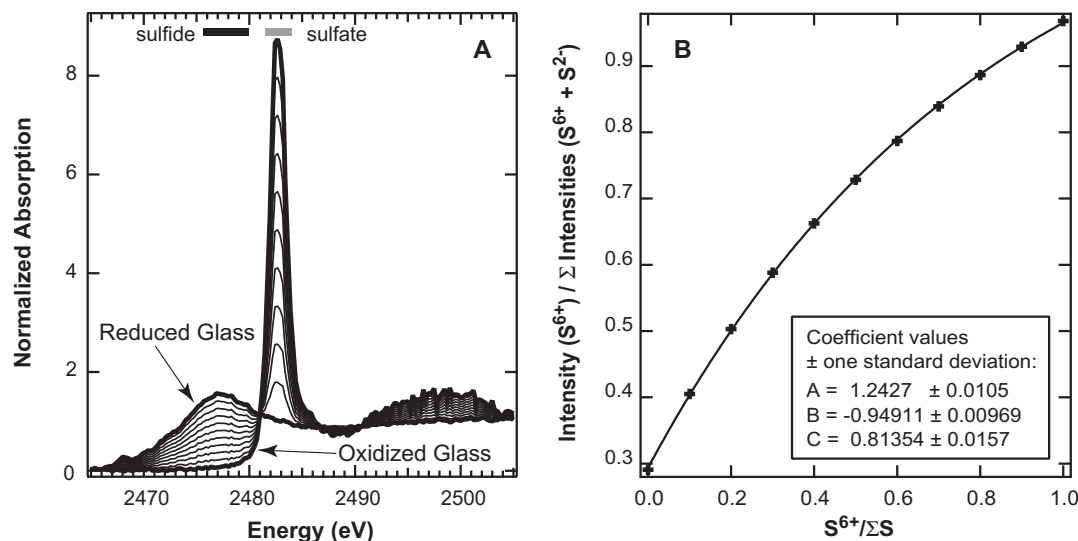


Fig. 8. Estimates of $S^{6+}/\Sigma S$ from XANES spectra. (A) The spectra of completely oxidized (SB-5) and completely reduced (SB-41) basaltic glasses used, respectively, as reference for $S^{6+}/\Sigma S = 1$ and $S^{6+}/\Sigma S = 0$ (bold curves). The thinner curves show the spectra of proportional combinations of the two end-members at 0.1 intervals of $S^{6+}/\Sigma S$. The shaded bands at the top of the figure illustrate the energy range used to calculate $I(S^{6+})$ and $I(S^{2-})$. (B) The relationship between $I(S^{6+})/\Sigma$ and $S^{6+}/\Sigma S$ for the spectra shown in (A). This relationship was used to calculate $S^{6+}/\Sigma S$ in samples showing combinations of S^{6+} and S^{2-} features (Tables 4 and 5).

glass (SB-5 and SB-41, with only S^{6+} or only S^{2-} present, respectively). The $I(S^{2-})$ and $I(S^{6+})$ parameters were determined from this calculated sequence and the trend of $I(S^{6+})$ over the sum of the two signals ($\Sigma I = I(S^{2-}) + I(S^{6+})$) was plotted against $S^{6+}/\Sigma S$ (Fig. 8B). In this protocol, we assume that mixtures of the two end-members match the spectra of samples with mixed oxidation state. Within the energy windows used for integration this assumption is valid as was checked by comparison. The trend in Fig. 8B was fitted by an exponential function:

$$S^{6+}/\Sigma S = -C * \ln\{[I(S^{6+})/\Sigma I - A]/B\} \quad (3)$$

where the fit parameters A , B , and C are 1.2427, -0.94911 , and 0.81354, respectively (Fig. 8B). This relationship can be used to estimate $S^{6+}/\Sigma S$ in samples showing S^{2-} and S^{6+} features in XANES spectra. For the samples synthesized in internally-heated pressure vessels, variation in fO_2 clearly results in systematic variations in the intensities of the sulfate and the sulfide features (increase in the intensity of the sulfate feature and decrease in the intensity of the sulfide feature, which are the basis for the model shown in Fig. 8A). These samples cover the complete range of $S^{6+}/\Sigma S$ (Table 4) as expected in the range of fO_2 used for this set of experiments. The natural samples for which XANES spectra showed coexistence of sulfide and sulfate species (Fig. 4–6) have well defined sulfide peaks with no discernible variations in the intensity of the sulfide features within each suite in the figures. The variation in $S^{6+}/\Sigma S$ is most noticeable in the variations in the sulfate feature because the intensity of the S^{6+} and S^{2-} have very different sensitivity per unit of $S^{6+}/\Sigma S$ as illustrated in Fig. 8A (i.e. minute changes in the concentration of S^{6+} will cause significant changes in the intensity of the sulfate feature but noticeable changes in the intensity of the sulfide feature requires larger

Table 4
Estimates of $S^{6+}/\Sigma S$ of synthetic basaltic samples from Eq. (3).

Spectrum	$I(S^{2-})$	$I(S^{6+})$	$I(S^{6+})/\Sigma I$	$S^{6+}/\Sigma S$ (%)
<i>Basaltic glasses (IHPV)</i>				
SB-5	0.52	15.62	0.97	100.83
SB-15	0.84	14.49	0.95	94.44
SB-19	1.02	14.38	0.93	91.33
SB-35	2.16	12.26	0.85	71.87
SB-6	3.99	7.93	0.67	40.41
SB-36	6.59	2.77	0.30	0.19
SB-41	6.27	2.57	0.29	-0.24

changes in the concentration of S^{2-}). In general the samples analyzed from Kilauea, and the Lamont and Loihi Seamounts are towards the reduced end of the $S^{6+}/\Sigma S$ range ($S^{6+}/\Sigma S < 0.3$) and have limited variation in $S^{6+}/\Sigma S$. However, it is significant that these samples show clear evidence of the presence of S^{6+} , in contrast to the samples from Juan de Fuca, Galapagos and the Lau Basin which are clearly dominated by S^{2-} with negligible S^{6+} (Table 5).

4.3. Changes in S speciation as a function of fO_2

As discussed by Wallace and Carmichael (1994), Matthews et al. (1999) and Métrich et al. (2009), the oxidation of S^{2-} to S^{6+} can be expressed as:



which can be rearranged as:

$$\log fO_2 = 0.5 \log((a[SO_4]^{2-})/(a[S]^{2-})) - 0.5 \log K \quad (5)$$

where K is the equilibrium constant (therefore a function of T and P) and $a[i]$ is the activity of component “ i ” in the sil-

Table 5
Estimates of $S^{6+}/\Sigma S$ of natural samples from Eq. (3).

Spectrum	I(S^{2-})	I(S^{6+})	I(S^{6+})/ ΣI	$S^{6+}/\Sigma S$ (%)
<i>Sulfide-dominated samples</i>				
Juan de Fuca D1-4G	6.57	3.02	0.31	1.84
Galapagos 1540-4	6.75	2.72	0.29	-0.53
Lau Basin 10-1-3-	6.96	2.68	0.28	-1.32
Lau Basin 20-5-1	6.50	2.52	0.28	-1.21
<i>Lamont Seamounts</i>				
1560-1843Z	5.76	3.81	0.40	9.51
1567-2019Z	5.89	3.82	0.39	9.05
1564-1857	6.27	3.63	0.37	6.49
F2-2	5.73	3.36	0.37	6.79
<i>Kilauea</i>				
Hw S508_6	4.49	5.25	0.54	24.32
Hw S508_1	5.62	4.62	0.45	14.76
Hw S508_2	4.99	4.45	0.47	16.86
Hw S508_4	5.46	4.32	0.44	13.77
Hw S508_3	5.55	4.29	0.44	13.22
Hw S508_5	5.80	3.77	0.39	9.08
<i>Loihi Seamount</i>				
KK-21-1	4.69	6.88	0.59	31.02
KK-19-21	4.57	6.25	0.58	28.90
KK-15-5	4.90	6.22	0.56	26.75
KK-29-10	5.07	4.93	0.49	19.19
KK-16-1	5.31	4.53	0.46	15.75
KK-15-4	6.31	2.45	0.28	-1.21

icate melt. Subtracting the $\log fO_2$ value for the FMQ buffer at the appropriate P - T conditions (written below as “ $\log(fO_2)_{FMQ}$ ”) so that fO_2 is expressed in terms of the

FMQ buffer and solving for $\log((a[SO_4]^{2-})/(a[S]^{2-}))$ we obtain:

$$\log((a[SO_4]^{2-})/(a[S]^{2-})) = 2\Delta FMQ + (\log K + 2\log(fO_2)_{FMQ}) \quad (6)$$

Eq. (4) defines a straight-line, $y = 2x + b$, with a slope of 2 and an intercept that is a function of the equilibrium constant and the reference FMQ buffer (as discussed by Matthews et al. (1999) and Métrich et al. (2009)). If the ratio of the activity coefficients does not deviate significantly from unity, then:

$$\log((a[SO_4]^{2-})/(a[S]^{2-})) \approx \log(S^{6+}/S^{2-}) \quad (7)$$

where (S^{6+}/S^{2-}) is the ratio of the S^{6+} and S^{2-} content.

Electron probe microanalysis provides data of total S and (using the method of Carroll and Rutherford (1988)) estimates of the proportion of S^{6+} species. Because most available data are expressed as $S^{6+}/\Sigma S$, the following conversion is needed to assess the fit of available data to the predicted linear trend:

$$(S^{6+}/S^{2-}) = (S^{6+}/\Sigma S)/(1 - (S^{6+}/\Sigma S)) \quad (8)$$

Fig. 9A shows $\log(S^{6+}/S^{2-})$ against ΔFMQ using the data compiled in Jugo et al. (2005b). The trend is essentially identical to that obtained by Matthews et al. (1999; see their Fig. 4) but we chose ΔFMQ for the abscissa to ease comparison with published S speciation diagrams. An arbitrary line with a slope of 2 was drawn passing through $S^{6+}/S^{2-} = 1$ at $fO_2 = FMQ + 1$ to evaluate the fit of the data obtained from EPMA (S K α shifts; Carroll and Rutherford, 1988)

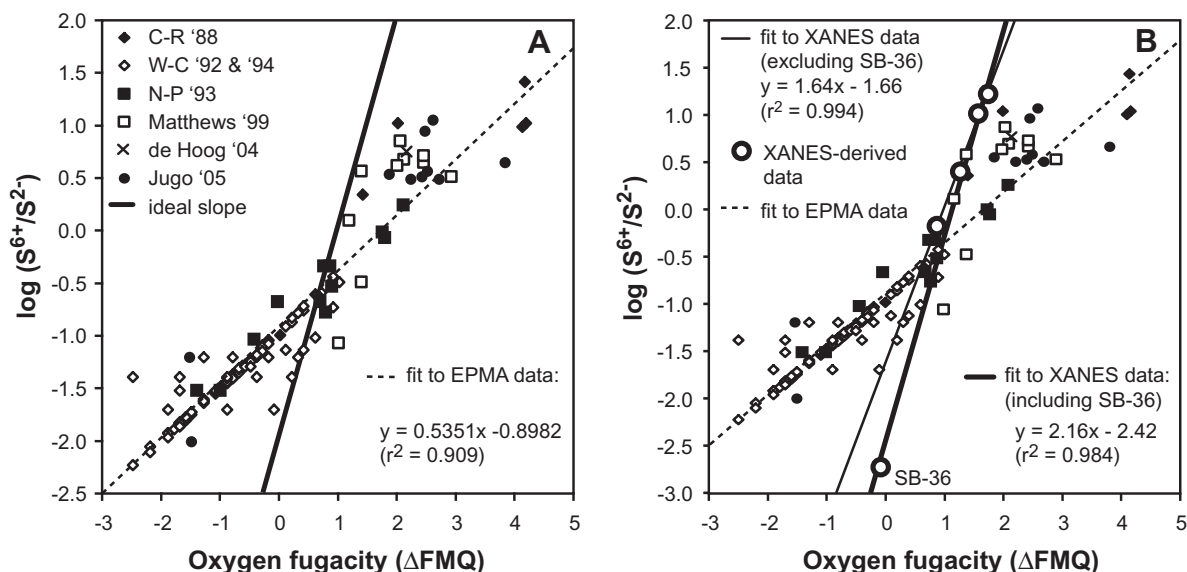


Fig. 9. $\log(S^{6+}/S^{2-})$ vs. ΔFMQ . (A) A compilation of data of samples with (S^{6+}/S^{2-}) estimated by EPMA. The dashed line is a linear regression to all data. The bold line has a slope = 2, as predicted by thermodynamic considerations and was arbitrarily passed through $\log(S^{6+}/S^{2-}) = 0.0$ at $\Delta FMQ = 1$ to illustrate the discrepancy of the available data with the expected slope. Data are from Carroll and Rutherford (1988), Wallace and Carmichael (1992, 1994); Nilsson and Peach (1993); Matthews et al. (1999), de Hoog et al. (2004); and Jugo et al. (2005a). Fig. 9B shows linear regressions to the XANES-derived data (solid lines) compared to the regression to the EMPA-derived data (shown in (A)). The bold line is the regression obtained through all the data. The thin solid line is the regression obtained if sample SB-36 is excluded in the regression.

with the slope predicted by Eq. (6). As discussed by Matthews et al. (1999) and Métrich et al. (2009) the compiled data (natural and experimental) show a large spread (especially at high fO_2) and define a general trend with a slope ($m = 0.5351$) significantly shallower than the slope ($m = 2$) predicted by Eq. (6). Two different processes, one affecting oxidized samples and the other affecting mostly reduced samples, could potentially explain the discrepancies. In the case of oxidized (S^{6+} -dominated) samples, photo-reduction during EPMA analysis to form S^{4+} (Wilke et al., 2008) explains why $\log(S^{6+}/S^{2-})$ in samples above FMQ + 1 is lower than expected (as shown in Jugo et al. (2005b)). In the case of reduced (S^{2-} -dominated) samples, electron exchange between Fe^{3+} and S^{2-} resulting in production of S^{6+} (as proposed by Métrich et al., 2009) explains why sulfide-dominated samples have more S^{6+} than predicted by Eq. (6).

Fig. 9B shows the fit to the XANES-derived data. Sulfur speciation (as S^{6+}/S^{2-}) was calculated from the parameters shown in Fig. 8B (Table 3; except for samples SB-5 and SB-41, which were used to define $S^{6+}/\Sigma S = 1$ and $S^{6+}/\Sigma S = 0$, respectively). A linear regression to the data (bold line) yields a slope ($m = 2.16$) closely matching the slope ($m = 2$) predicted by Eq. (6). The regression is heavily influenced by sample SB-36. If sample SB-36 is not included in the regression (thin solid line) the slope ($m = 1.64$) is not as close to the theoretical value but still significantly better than the fit obtained for the EPMA-derived data. This close match implies that S oxidation during quenching (as suggested by Métrich et al. (2009)) did not occur and, therefore, the $S^{6+}/\Sigma S$ can be preserved (at least for the samples synthesized in internally-heated pressure vessels equipped with a rapid-quench system). Moreover, only the small sulfate-related feature observed in Fig. 2 for the Juan de Fuca sample could be interpreted as product of electron exchange between S and Fe. The lack of such feature in the basaltic samples from the Galapagos spreading center or the Lau Basin, indicate that, if it indeed happens, not all natural basalts undergo such electron exchange on quenching. Unless the quench rate of the glasses from Juan de Fuca glass is significantly different than the quench rate of the Galapagos or Lau Basin glasses (or the rest of the natural samples) one can conclude that the Juan de Fuca glass quenched from a melt at relatively more oxidizing conditions.

Fig. 10A compares the $S^{6+}/\Sigma S$ vs. ΔFMQ curves derived from XANES data with the curve derived from EPMA (Jugo et al., 2005b). The new curves (solid lines in Fig. 10A) were constructed using a function derived by combining Eqs. (6) and (8):

$$S^{6+}/\Sigma S = 1/(1 + 10^{(A-B\Delta FMQ)}) \quad (9)$$

where “ A ” is the translation parameter that controls the position of the curve along the ΔFMQ axis, and “ B ” is a scaling parameter that controls the steepness of the sigmoidal curve (which correspond to the slope of the lines shown in Fig. 9). Two sets of parameters were obtained for Eq. (9). The first set (bold line in Fig. 10A) was obtained by forcing B to be equal to 2 (as predicted from the theoretical considerations summarized by Eq. (6)). Coefficient “ A ” for this approach was $A = 2.1 \pm 0.1$ ($\chi^2 = 0.007$). The second set (thin solid line

in Fig. 10A) did not put any constraints for coefficient “ A ”, resulting in $A = B = 1.6 \pm 0.1$ ($\chi^2 = 0.001$). The results were essentially identical (within error) regardless of whether sample SB-36 was or not included because the curves were forced (by definition) to vary between $S^{6+}/\Sigma S = 0$ and $S^{6+}/\Sigma S = 1$. As shown in Fig. 10A, the two curves essentially overlap each other (except for a small gap between FMQ and FMQ + 1). Because the results are consistent with the predictions of equation 4, the best parametrization for $S^{6+}/\Sigma S$ as a function of fO_2 can be expressed as:

$$S^{6+}/\Sigma S = 1/(1 + 10^{(2.1-2\Delta FMQ)}) \quad (10)$$

The curve predicts: (a) an even narrower interval for the change from S^{2-} to S^{6+} than the curve derived from EPMA data (from $S^{6+}/\Sigma S = 0.1$ to $S^{6+}/\Sigma S = 0.9$ in slightly less than 1 log unit, rather than 2 log units), and (b) higher $S^{6+}/\Sigma S$ at lower fO_2 above FMQ + 1. This has significant implication for S behavior in magmatic systems because as shown in Fig. 10B the range in fO_2 for the transition from S^{2-} to S^{6+} overlaps the range in fO_2 at which arc magmas are thought to be generated (Parkinson and Arculus, 1999) and the fO_2 estimated for island-arc basalts (IAB), ocean island basalts (OIB), and backarc basin basalts (BABB) erupted on the seafloor (Ballhaus, 1993).

4.4. Sulfur content at sulfide saturation as a function of fO_2

As shown in Jugo (2009) variations in $S^{6+}/\Sigma S$ above $fO_2 = FMQ$ drastically affect how S behaves in magmatic systems because the presence of S^{6+} in a silicate melt enhances the S content at sulfide saturation (SCSS), meaning that as fO_2 increases (and S^{6+} becomes dominant) SCSS will increase exponentially hampering the saturation of sulfide phases and potentially dissolving any sulfides present. This is consistent, for example, with the hypothesis of Sisson (2003) for the occurrence of native gold in a sample of Kilauea basanite (from the same suite of samples shown here in Fig. 5). Sisson (2003) explained the presence of native Au in the basanite as a residue from resorption of a Au-bearing sulfide entrained in the melt. Fig. 11 shows the expected increase in SCSS calculated from the curves shown in Fig. 10. As shown in Jugo (2009):

$$SCSS = [S^{2-}]/(1 - (S^{6+}/\Sigma S)) \quad (11)$$

Substituting (10) in (11) and rearranging the resulting expression to its simplest form, we obtain:

$$SCSS = [S^{2-}](1 + 10^{(2\Delta FMQ - 2.1)}) \quad (12)$$

The S content when only S^{2-} is present, $[S^{2-}]$ depend on many parameters (e.g., T , P , and FeO content in the melt; Haughton et al., 1974; Wendlandt, 1982). For basaltic melts at P , and T appropriate for subduction zones (for example) $[S^{2-}]$ is about 0.15 wt% (Jugo et al., 2005a); this value represents the SCSS for reduced samples at any fO_2 for which sulfate species in the melt are negligible. The exponential increase in SCSS is determined by the increase in $S^{6+}/\Sigma S$ with increasing fO_2 and it is limited by the fO_2 at which a sulfate phase (e.g., crystalline anhydrite) saturates the melt (otherwise the exponential increase in SCSS would tend to infinite). For the curves shown in figure (11) the S content at

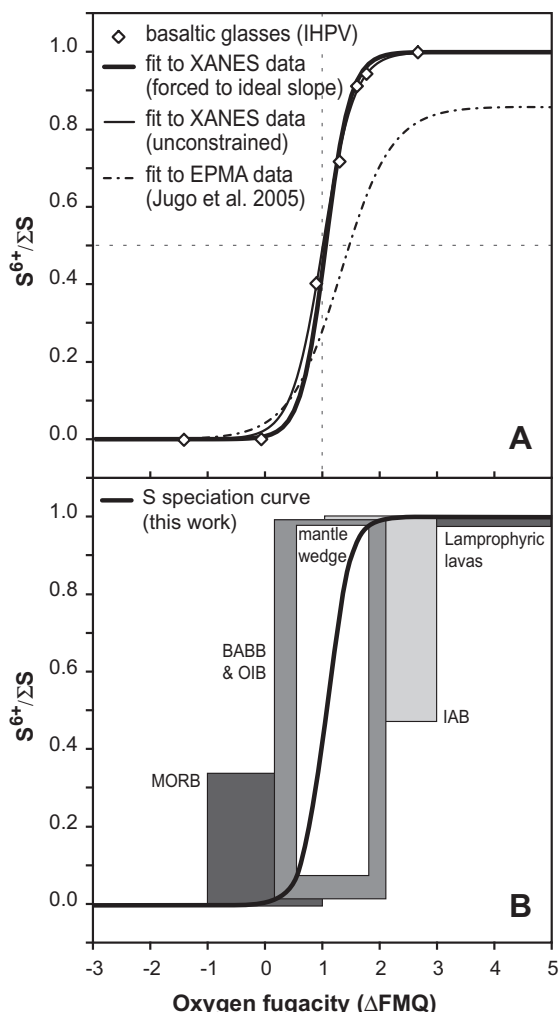


Fig. 10. Sulfur speciation curve vs. fO_2 derived from the $S^{6+}/\Sigma S$ estimates of XANES data for basaltic glasses (in bold) synthesized in internally-heated pressure vessels. (A) is a comparison of the empirical $S^{6+}/\Sigma S$ vs. fO_2 curve derived from data obtained by EPMA (dashed line; Jugo et al., 2005b) and the $S^{6+}/\Sigma S$ vs. fO_2 curve derived from XANES-derived data (diamond-shaped symbols). The bold curve is the curve obtained if the curve is forced to match the slope predicted in equation 1. The thinner line is the fit for an unconstrained slope. (B) Fields from different tectonic settings and magma types are shown overlapping the $S^{6+}/\Sigma S$ vs. fO_2 curve to highlight the relevance of variations in S^{6+}/S^{2-} in natural systems. Oxygen fugacity range for mid-ocean ridge basalts (MORB: $FMQ - 1$ to $FMQ + 1$), back-arc basin basalts (BABB: FMQ to $FMQ + 2$), ocean island basalts (OIB: same range as BABB), island-arc basalts (IAB: $FMQ = 1$ to $FMQ + 3$), the mantle wedge above subduction zones where partial melting occurs ($FMQ + 0.5$ to $FMQ + 1.4$), and lamprophyric lavas from Mexico ($\sim FMQ + 3$ to $FMQ + 5$) are from Ballhaus (1993), Parkinson and Arculus (1999), and Carmichael (1991). The height (and vertical position) of each field was defined by the intersection of the curve with the estimated fO_2 range and provide a visual indication of the range in $S^{6+}/\Sigma S$ expected in each type of magma.

sulfate saturation, $[S] = 1.2$ wt% was used based on the data from Jugo et al. (2005a) for experiments at 1300 °C and 1 GPa. Thus, the curves shown mostly represent conditions expected during partial melting. As shown by Luhr

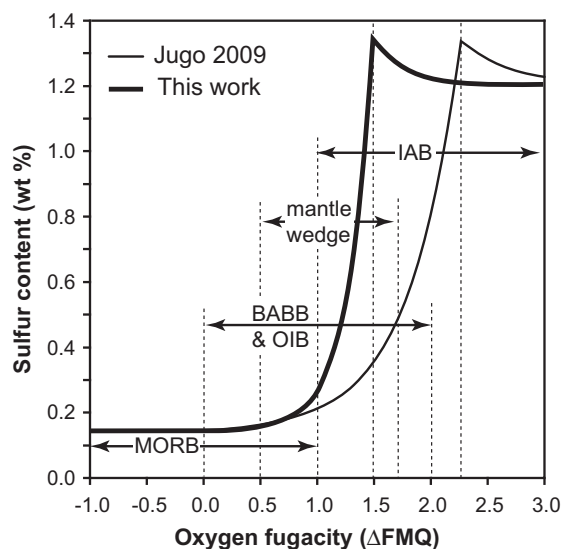


Fig. 11. Sulfur content at sulfide saturation (SCSS; exponentially increasing curves) and sulfur content at “anhydrite” (sulfate) saturation (SCAS) as predicted by the model derived by Jugo (2009) and comparing the curve derived from EPMA (thinner line) and the curve derived from the XANES-derived data (bold line). The fO_2 of the fields shown in Fig. 10 are shown for reference. The expected exponential increase in SCSS with increasing fO_2 is steeper (happening over a narrower fO_2 range) than estimated with the model based on S speciation estimated by EPMA. The most significant aspect of this model is that it indicates that only reduced magmas (i.e. MORB) are dominated by sulfide species and S behavior, in particular SCSS, in all other environments may change significantly with small variations in fO_2 .

(1990), the contrast between SCSS and SCAS (for the end-members; i.e. sulfide-dominated and sulfate-dominated) depends mostly on changes in SCAS, which is a function of P and T (SCAS increases linearly with increasing P and exponentially with increasing T). Thus, for silicate melts at lower P and T (or more felsic in composition) the exponential growth will still exist but the maximum SCSS will be lower and sulfate saturation should occur at lower fO_2 (see Jugo, 2009, for example, for a comparison between the relative behavior between basalts at 1300 °C and 1 GPa and trachyandesites at 1025 °C and 200 MPa). In any case, the recalculated SCSS curve shows an even steeper curve with increasing fO_2 , such that at $fO_2 > FMQ + 1$ basaltic melts are capable of transporting much larger amounts of S than reduced (e.g., typical MORB) basalts (which also implies that lower degrees of partial melting would be required to eliminate sulfides present in the melt source).

5. CONCLUSIONS

XANES analysis of natural samples showed that basalts from spreading centers (e.g., Lau Basin, Galapagos) are dominated by S^{2-} with little or no detectable S^{6+} . Analysis of samples from arc magmas (e.g., Cascades, Pinatubo) show that dissolved S^{6+} dominated in those magmas, with essentially no detectable S^{2-} in the samples. This does not imply that S^{2-} is not present in arc magmas because the

samples analyzed are from the most oxidized samples available to us (De Hoog et al., 2004; Rowe et al., 2007). Samples from ocean island basalts and basanites (Kilauea, Loihi, Lamont) show that these magmas contain variable proportions of S^{2-} and S^{6+} , which is consistent with estimates of the fO_2 of plume-related magmas indicating that the range in fO_2 of ocean island basalts is intermediate between MORB and arc magmas (Ballhaus, 1993). If variable $S^{6+}/\Sigma S$ is a feature relatively common to plume-related magmatism it may have significant implications for the behavior of S (and as consequence chalcophile and siderophile elements) in those systems. XANES spectra from basaltic glasses synthesized in internally-heated pressure vessels also showed variable proportions of S^{2-} and S^{6+} . The relationship between $S^{6+}/\Sigma S$ and fO_2 (as ΔFMQ) indicates that $S^{6+}/\Sigma S$ were not significantly affected during quenching. We found no evidence for S^{4+} species, further confirming that sulfite is mostly an analytical artifact (Wilke et al., 2008) or restricted to specific melt compositions (Métrich et al., 2009). Thus, it can be safely concluded that S^{4+} is not relevant to natural systems. Photo-reduction of S^{6+} to S^{4+} during microprobe analysis is most likely the cause of the discrepancy between the $S^{6+}/\Sigma S$ vs. fO_2 curves derived from EPMA data and XANES data (the EPMA data showing a significant deviation from theoretical constraints and the XANES-derived data closely matching them). Improvement of the EPMA technique would require characterization of glass samples analyzed by XANES and revision of analytical protocols to minimize photo-reduction during analysis by minimizing exposure time and probe current density (Morgan and London, 2005). The approach used by Vigouroux et al. (2008) for example, using 15 kV, 30 nA, 5 μm beam diameter (for a probe current density of ~ 1.5 nA/ mm^2) and moving the beam every 20 s seems to minimize the photo-reduction problem (they were able to obtain $S^{6+}/\Sigma S$ values up to 0.95). The XANES spectra shown here and the results of our modeling emphasize the importance of estimating $S^{6+}/\Sigma S$ to assess the geochemical behavior of S in arc magmas, in particular to estimate the amount of S that can be transported by silicate melts and the conditions that allow sulfide precipitation. A refinement of the model of Jugo (2009) for the changes in SCSS with increasing fO_2 (Fig. 11) indicates that changes in fO_2 above $FMQ + 1$ will strongly affect the S content required to saturate an immiscible sulfide melt in basaltic magmas and in silicate melts in general.

ACKNOWLEDGMENTS

We would like to thank all the researchers who provided natural samples for XANES analysis: Keiko Hattori (University of Ottawa) and Cees-Jan de Hoog (Göteborg University, Sweden) for Pinatubo samples; Mike Rowe (University of Texas) for Cascades samples; Paul Wallace (University of Oregon) for samples from several localities including: Lamont Seamounts, Loihi Seamount, Galapagos Spreading Center and Lau Basin; T. Sisson (USGS) for samples from Kilauea, Hawaii. We also thank Lauren Cooper, Jennifer Wade, and Terry Plank (Boston University) who provided melt inclusion samples in olivine from the Tonga Volcanic Arc and Augustine volcano. Those samples proved difficult to analyze because of their small volume, and were not included in the results. We thank Jean Susini,

Muriel Salomé and Marine Cotte from Beamline ID21 at the ESRF for their expertise and assistance during collection of the XANES data. We thank Dr. Bruno Scaillet, Dr. Guil Mallmann, and an anonymous peer for their detailed reviews. This project benefited from funds provided by DFG (Germany) and NSERC (Canada) and beamtime provided by the ESRF.

REFERENCES

- Alard O., Griffin W. L., Lorand J. P., Jackson S. E. and O'Reilly S. Y. (2000) Non-chondritic distribution of the highly siderophile elements in mantle sulphides. *Nature* **407**, 891–894.
- Backnaes L., Stelling J., Behrens H., Goettlicher J., Mangold S., Verheijen O., Beerkens R. G. C. and Deubner J. (2008) Dissolution mechanisms of tetravalent sulphur in silicate melts: evidence from sulphur K edge XANES studies on glasses. *J. Am. Ceram. Soc.* **91**, 721–727.
- Ballhaus C. (1993) Redox States of Lithospheric and Asthenospheric Upper-Mantle. *Contrib. Mineral. Petrol.* **114**, 331–348.
- Berndt J., Liebske C., Holtz F., Freise M., Nowak M., Ziegenbein D., Hurkuck W. and Koepke J. (2002) A combined rapid-quench and H_2 -membrane setup for internally heated pressure vessels: description and application for water solubility in basaltic melts. *Am. Mineral.* **87**, 1717–1726.
- Botcharnikov R. E., Koepke J., Holtz F., McCammon C. and Wilke M. (2005) The effect of water activity on the oxidation and structural state of Fe in a ferro-basaltic melt. *Geochim. Cosmochim. Acta* **69**, 5071–5085.
- Campbell I. H., Czamanske G. K., Fedorenko V. A., Hill R. I. and Stepanov V. (1992) Synchronism of the Siberian Traps and the Permian–Triassic boundary. *Science* **258**, 1760–1763.
- Carmichael I. S. E. (1991) The redox states of basic and silicic magmas – a reflection of their source regions. *Contrib. Mineral. Petrol.* **106**, 129–141.
- Carroll M. R. and Rutherford M. J. (1985) Sulfide and sulfate saturation in hydrous silicate melts. *J. Geophys. Res.* **90**, C601–C612.
- Carroll M. R. and Rutherford M. J. (1987) The stability of igneous anhydrite: experimental results and implications for S behavior in the 1982 El Chichón trachyandesite and other evolved magmas. *J. Petrol.* **28**, 781–801.
- Carroll M. R. and Rutherford M. J. (1988) Sulfur speciation in hydrous experimental glasses of varying oxidation state: results from measured wavelength shifts of sulfur X-rays. *Am. Mineral.* **73**, 845–849.
- Carroll, M. R. and Webster J. D. (1994) Solubilities of sulfur, noble gases, nitrogen, chlorine, and fluorine in magmas. In *Volatiles in Magmas* (eds. M. R. Carroll and J. R. Holloway), vol. 30. Mineralogical Society of America, Reviews in Mineralogy, pp. 231–279.
- Churakov S. V. and Gottschalk M. (2003) Perturbation theory based equation of state for polar molecular fluids: II. Fluid mixtures. *Geochim. Cosmochim. Acta* **67**, 2415–2425.
- Clemente B., Scaillet B. and Pichavant M. (2004) The solubility of sulphur in rhyolitic melts. *J. Petrol.* **45**, 2171–2196.
- De Hoog J. C. M., Hattori K. H. and Hoblitt R. P. (2004) Oxidized sulfur-rich mafic magma at Mount Pinatubo, Philippines. *Contrib. Mineral. Petrol.* **146**, 750–761.
- Fleet M. E. (2005) XANES spectroscopy of sulfur Earth materials. *Can. Mineral.* **43**, 1811–1838.
- Fleet M. E., Liu X., Harmer S. L. and King P. L. (2005) Sulfur K-edge XANES spectroscopy: chemical state and content of sulfur in silicate glasses. *Can. Mineral.* **43**, 1605–1618.
- Hart S. R. and Gaetani G. A. (2006) Mantle Pb paradoxes: the sulfide solution. *Contrib. Mineral. Petrol.* **152**, 295–308.

- Haughton D. R., Roeder P. L. and Skinner B. J. (1974) Solubility of sulfur in mafic magmas. *Econ. Geol.* **69**, 451–467.
- Jayasuriya K. D., O'Neill H. St. C., Berry A. J. and Campbell S. J. (2004) A Moessbauer study of the oxidation state of Fe in silicate melts. *Am. Mineral.* **89**, 1597–1609.
- Jugo P. J. (2009) Sulfur content at sulfide saturation in oxidized magmas. *Geology* **37**, 415–418.
- Jugo P. J., Luth R. W. and Richards J. P. (2005a) An experimental study of the sulfur content in basaltic melts saturated with immiscible sulfide or sulfate liquids at 1300 °C and 1.0 GPa. *J. Petrol.* **46**, 783–798.
- Jugo P. J., Luth R. W. and Richards J. P. (2005b) Experimental data on the speciation of sulfur as a function of oxygen fugacity in basaltic melts. *Geochim. Cosmochim. Acta* **69**, 497–503.
- Li D., Bancroft G. M., Kasrai M., Fleet M. E., Feng X. H. and Tan K. H. (1995) S K- and L-edge X-ray absorption spectroscopy of metal sulfides and sulfates: applications in mineralogy and geochemistry. *Can. Mineral.* **33**, 949–960.
- Li C. and Ripley E. M. (2009) Sulfur contents at sulfide-liquid or anhydrite saturation in silicate melts: empirical equations and example applications. *Econ. Geol.* **104**, 405–412.
- Liu Y., Samaha N.-T. and Baker D. R. (2007) Sulfur concentration at sulfide saturation (SCSS) in magmatic silicate melts. *Geochim. Cosmochim. Acta* **71**, 1783–1799.
- Luhr J. F. (1990) Experimental phase-relations of water-saturated and sulfur-saturated arc magmas and the 1982 eruptions of El Chichon Volcano. *J. Petrol.* **31**, 1071–1114.
- Matthews S. J., Moncrieff D. H. S. and Carroll M. R. (1999) Empirical calibration of the sulfur valence oxygen barometer from natural and experimental glasses: methods and applications. *Miner. Mag.* **63**, 421–431.
- Mavrogenes J. A. and O'Neill H. S. C. (1999) The relative effects of pressure, temperature and oxygen fugacity on the solubility of sulfide in mafic magmas. *Geochim. Cosmochim. Acta* **63**, 1173–1180.
- McKeown D. A., Muller I. S., Gan H., Pegg I. L. and Stolte W. C. (2004) Determination of sulfur environments in borosilicate waste glasses using X-ray absorption near-edge spectroscopy. *J. Non-Cryst. Solids* **333**, 74–84.
- Métrich N., Berry A. J., O'Neill H. St. C. and Susini J. (2009) The oxidation state of sulfur in synthetic and natural glasses determined by X-ray absorption spectroscopy. *Geochim. Cosmochim. Acta* **73**, 2382–2399.
- Métrich N., Bonnin-Mosbah M., Susini J., Menez B. and Galois L. (2002) Presence of sulfite (S-IV) in arc magmas: implications for volcanic sulfur emissions. *Geophys. Res. Lett.*, v. 29.
- Mitchell R. H. and Keays R. R. (1981) Abundance and distribution of gold, palladium and iridium in some spinel and garnet lherzolites – implications for the nature and origin of precious metal-rich intergranular components in the upper mantle. *Geochim. Cosmochim. Acta* **45**, 2425–2442.
- Morgan G. B. and London D. (2005) Effect of current density on the electron microprobe analysis of alkali aluminosilicate glasses. *Am. Mineral.* **90**, 1131–1138.
- Moune S., Holtz F. and Botcharnikov R. (2009) Sulphur solubility in andesitic to basaltic melts: implications for Hekla volcano. *Contrib. Mineral. Petrol.* **157**, 691–707.
- Nilsson K. and Peach C. L. (1993) S speciation, oxidation state, and S concentration in back-arc magmas. *Geochim. Cosmochim. Acta* **57**, 3807–3813.
- O'Neill H. St. C. and Mavrogenes J. A. (2002) The sulfide capacity and sulfur content at sulfide saturation of silicate melts at 1400 °C and 1 bar. *J. Petrol.* **43**, 1049–1087.
- Paris E., Giuli G., Carroll M. R. and Davoli I. (2001) The valence and speciation of sulfur in glasses by X-ray absorption spectroscopy. *Can. Mineral.* **39**, 331–339.
- Parkinson I. J. and Arculus R. J. (1999) The redox state of subduction zones: insights from arc-peridotites. *Chem. Geol.* **160**, 409–423.
- Rampino M. R. and Self S. (1992) Volcanic winter and accelerated glaciation following the toba super-eruption. *Nature* **359**, 50–52.
- Rehkamper M., Halliday A. N., Fitton J. G., Lee D. C., Wieneke M. and Arndt N. T. (1999) Ir, Ru, Pt and Pd in basalts and komatiites: new constraints for the geochemical behavior of the platinum-group elements in the mantle. *Geochim. Cosmochim. Acta* **63**, 3915–3934.
- Reichow M. K., Pringle M. S., Al'Mukhamedov A. I., Allen M. B., Andreichev V. L., Buslov M. M., Davies C. E., Fedoseev G. S., Fitton J. G., Inger S., Medvedev A. Y., Mitchell C., Puchkov V. N., Safonova I. Y., Scott R. A. and Saunders A. D. (2009) The timing and extent of the eruption of the Siberian Traps large igneous province: implications for the end-Permian environmental crisis. *Earth Planet. Sci. Lett.* **277**, 9–20.
- Renne P. R., Zhang Z. C., Richards M. A., Black M. T. and Basu A. R. (1995) Synchrony and causal relations between Permian–Triassic boundary crises and Siberian Flood volcanism. *Science* **269**, 1413–1416.
- Rowe M. C., Kent A. J. R. and Nielsen R. L. (2007) Determination of sulfur speciation and oxidation state of olivine hosted melt inclusions. *Chem. Geol.* **236**, 303–322.
- Roy-Barman M., Wasserburg G. J., Papanastassiou D. A. and Chaussidon M. (1998) Osmium isotopic compositions and Re–Os concentrations in sulfide globules from basaltic glasses. *Earth Planet. Sci. Lett.* **154**, 331–347.
- Self S., Zhao J., Holasek R. E., Torres R. C. and King A. J. (1996) The atmospheric impact of the 1991 Mount Pinatubo eruption. In *Fire and Mud: Eruptions and Lahars of Mount Pinatubo, Philippines* (eds. C. G. Newhall and R. S. Punongbayan). Philippine Institute of Volcanology and Seismology/University of Washington Press, Quezon City/Seattle, pp. 1098–1115.
- Shishkina T. A., Botcharnikov R. E., Holtz F., Almeev R. R., and Portnyagin M. V. (in press) Solubility of H₂O and CO₂-bearing fluids in tholeiitic basalts at pressures up to 500 MPa. *Chem. Geol.* doi:10.1016/j.chemgeo.2010.07.014.
- Sisson T. W. (2003) Native gold in a Hawaiian alkalic magma. *Econ. Geol.* **95**, 643–648.
- Susini J., Salomé M., Fayard B., Ortega R. and Kaulich B. (2002) The scanning X-ray microprobe at the ESRF “X-ray Microscopy” beamline. *Surf. Rev. Lett.* **9**, 203–211.
- Symonds R. B., Rose W. I., Bluth G. J. S. and Gerlach T. M. (1994) Volcanic-gas studies: Methods, results, and applications. In *Volatiles in Magmas* (eds. M. R. Carroll and J. R. Holloway), vol. 30. Mineralogical Society of America, Reviews in Mineralogy, pp. 1–66.
- Vigouroux N., Wallace P. J. and Kent A. J. R. (2008) Volatiles in high-K magmas from the western Trans-Mexican volcanic belt: evidence for fluid fluxing and extreme enrichment of the mantle wedge by subduction processes. *J. Petrol.* **49**, 1589–1618.
- Wallace P. J. and Carmichael I. S. E. (1992) Sulfur in basaltic melts. *Geochim. Cosmochim. Acta* **56**, 1863–1874.
- Wallace P. J. and Carmichael I. S. E. (1994) S-speciation in submarine basaltic glasses as determined by measurements of SK-alpha X-ray wavelength shifts. *Am. Mineral.* **79**, 161–167.
- Wendlandt R. F. (1982) Sulfide saturation of basalt and andesite melts at high pressures and temperatures. *Am. Mineral.* **67**, 877–885.
- Wilke M., Jugo P. J., Klimm K., Susini J., Botcharnikov R., Kohn S. C. and Janousch M. (2008) The origin of S⁴⁺ detected in silicate glasses by XANES. *Am. Mineral.* **93**, 235–240.